HHS Public Access

Author manuscript

Biochem Pharmacol. Author manuscript; available in PMC 2017 February 01.

Published in final edited form as:

Biochem Pharmacol. 2016 September 15; 116: 22–38. doi:10.1016/j.bcp.2016.06.019.

Platinum-containing compound platinum pyrithione is stronger and safer than cisplatin in cancer therapy

Chong Zhao[#a], **Xin Chen**[#a], **Dan Zang**[a], **Xiaoying Lan**[a], **Siyan Liao**[a], **Changshan Yang**[a], **Peiquan Zhang**[a], **Jinjie Wu**[a], **Xiaofen Li**[a], **Ningning Liu**[a,b], **Yuning Liao**[a], **Hongbiao Huang**[a], **Xianping Shi**[a], **Lili Jiang**[a], **Xiuhua Liu**[c,d], **Zhimin He**[e], **Xuejun Wang**[a,f,*], and **Jinbao Liu**[a,*]

[a]State Key Lab of Respiratory Disease, Protein Modification and Degradation Lab, Department of Pathophysiology, Guangzhou Medical University, Guangdong, China

[b]Guangzhou Research Institute of Cardiovascular Disease, The Second Affiliated Hospital, Guangzhou Medical University, Guangzhou, Guangdong 510260, China

[c]Institute of Environmental and Analytical Sciences, College of Chemistry and Chemical Engineering, Henan University, Kaifeng, Henan 475004, China

[d]Key Lab of Natural Drug and Immune Engineering of Henan Province, Kaifeng, Henan 475004, China

[e]Cancer Hospital and Cancer Research Institute, Guangzhou Medical University, Guangzhou, Guangdong 510095, China

[f]Division of Basic Biomedical Sciences, Sanford School of Medicine of the University of South Dakota, Vermillion, SD 57069, USA

[#] These authors contributed equally to this work.

Abstract

DNA is the well-known molecular target of current platinum-based anticancer drugs; consequently, their clinical use is severely restricted by their systemic toxicities and drug resistance originating from non-selective DNA damage. Various strategies have been developed to circumvent the shortcomings of platinum-based chemotherapy but the inherent problem remains unsolved. Here we report that platinum pyrithione (PtPT), a chemically well-characterized synthetic complex of platinum, inhibits proteasome function and thereby exhibits greater and more selective cytotoxicity to multiple cancer cells than cisplatin, without showing discernible DNA damage both *in vitro* and *in vivo*. Moreover, unlike the classical proteasome inhibitor bortezomib/Velcade which inhibits the proteasome via blocking the peptidase activity of 20S proteasomes,

[*]Corresponding authors at: Division of Basic Biomedical Sciences, Sanford School of Medicine of the University of South Dakota, Vermillion, SD 57069, USA (X. Wang), Protein Modification and Degradation Lab, Department of Pathophysiology, Guangzhou Medical University, Guangzhou, Guangdong 510182, China (J. Liu). xuejun.wang@usd.edu (X. Wang), jliu@gzhmu.edu.cn (J. Liu). .

Competing financial interests

The authors declare that they have no competing commercial or financial interests.

Author contributions

J.L., C.Z. and X.W. designed experiments; C.Z., X.C., D.Z., X. Lan, C. Y., J. Wu, Y. Liao, H.H., L.J., X.S., and X.L. performed experiments; S. Liao and P.Z performed computational docking; X. Li and L.N. provided clinical samples; J.L. and X.W. wrote the manuscript. All authors reviewed the manuscript.

PtPT primarily deactivates 26S proteasome-associated deubiquitinases USP14 and UCHL5. Furthermore, PtPT can selectively induce cytotoxicity and proteasome inhibition in cancer cells from leukemia patients but not peripheral blood mononuclear cells from healthy humans. In nude mice, PtPT also remarkably inhibited tumor xenograft growth, without showing the adverse effects that were induced by cisplatin. Hence, we have discovered a new platinum-based anti-tumor agent PtPT which targets 26S proteasome-associated deubiquitinases rather than DNA in the cell and thereby exerts safer and more potent anti-tumor effects, identifying a highly translatable new platinum-based anti-cancer strategy.

Keywords

DNA damage; Platinum pyrithione; Proteasome; Deubiquitinases; Tumor

1. Introduction

Chemotherapy using cisplatin, the platinum coordination complex cis-diamminedichloroplatinum (II) (CDDP), is a prevailing paradigm for the use of metal medicine in cancer treatment [1]. However, severe side effects resulting from the poor specificity of cisplatin and the acquired or intrinsic resistance to cisplatin significantly restrict its clinical use and efficacy against various cancers [2]. Cisplatin interacts with DNA by the N7 site of guanine and ade-nine bases, forming DNA adducts, and thereby interfering with DNA replication and transcription [3], which constitutes the primary biochemical mechanism of cisplatin's powerful anti-tumor effects but non-discriminatively targeting DNA by cisplatin also causes severe consequences to normal cells, yielding serious adverse effects and limiting its use. The limitations of cisplatin have stimulated intensive search for additional platinum-based anticancer drugs. For example, carboplatin and oxaliplatin are two of FDA-approved platinum-based drugs with somewhat improved therapeutic properties but they all operate via a similar non-specific mechanism of action; therefore, they retain most of the undesirable effects of cisplatin [4].

With the growing understanding of the molecular biology of the ubiquitin–proteasome system (UPS) and the success in clinical use of proteasome inhibitors (e.g., bortezomib, carfilzomib) to treat multiple myeloma, proteasome inhibition has proven to be an attractive strategy for cancer therapy [5]. The UPS consists of three main components including the ubiquitin-conjugating system, the deubiquitinating enzymes (DUBs), and the proteasome [6,7]. Since the UPS is the pivot of protein degradation, deubiquitination of tagged proteins by DUBs is essential for regulating proteasome-mediated degradation, and has been implicated in the pathogenesis of many human diseases, including cancer [8]. Unlike 20S proteasome inhibitor, most of reported DUB inhibitors can specifically target one or several DUBs by which distinctive proteins are regulated. Interference with the ubiquitin deconjugation may generate more specific and less toxic anticancer agents.

The human genome encodes 98 putative DUBs [9]. Three of them, including USP14, UCHL5 and RPN11 are known to associate with the 26S proteasome (26S). USP14 and UCHL5 are cysteine proteases, belonging to the ubiquitin-specific protease (USP) and the

ubiquitin C-terminal hydrolase (UCH) families, respectively. RPN11 or POH1 is a metalloprotease, belonging to the JAMM domain family of DUBs. These DUBs edit polyubiquitin chains on proteasome substrates for protein degradation [10,11]. Due to the great potential for DUBs to become therapeutic targets in cancer, several small molecule inhibitors and natural compounds have been developed. Some of these inhibitors are broad spectrum, while others are very specific, targeting only a particular DUB. Several DUB inhibitors have emerged from preclinical testing [12].

In the present study, we have identified a new platinum-based anti-tumor agent PtPT which targets 26S proteasome-associated DUBs rather than DNA in the cell and thereby exerts safer and potent anti-tumor effects; hence, a highly promising and easily translatable new platinum-based anti-cancer strategy is experimentally demonstrated.

2. Materials and methods

2.1. Cell culture

K562 (chronic myelogenous leukemia), HEK293 (human embryonic epithelial cells), U266 (myeloma cells), SMMC-7721 (Human hepatoma cells), 16HBE (non-transformed bronchial epithelial cells) and L02 (normal liver cells) were purchased from American Type Culture Collection (Manassas, VA, USA), A549 and cisplatin-resistant A549/DDP were a gift of Dr. Z. He (Cancer Hospital and Cancer Research Institute of Guangzhou Medical University). Most of cell lines were grown in RPMI 1640 (*Gibco*-Invitrogen, Carlsbad, CA, USA) supplemented with 10% FBS, 100 units/ml of penicillin and 100 g/ml of streptomycin. A549/DDP cells were routinely maintained in the same medium but in the presence of 1.5 μg/ml cisplatin, which was removed before experiments were started by a wash-out period of 2–3 days. HEK293 cultured in DMEM medium with high glucose supplemented with 10% fetal bovine serum (HyClone, Logan, UT, USA). GFPu, a green fluorescence protein (GFP) modified by carboxyl fusion of degron CL1, was previously proven a specific surrogate substrate for the UPS [13]. HEK-293 cells stably harboring GFPu were created as we previously described [14].

2.2. Blood samples and isolation of peripheral blood monocytes

Peripheral blood samples of normal controls were obtained from Guangzhou Blood Center and peripheral bone marrow samples of AML patients were obtained from discarded material utilized for routine laboratory tests at the Department of Hematology, Guangzhou First Municipal People's Hospital of Guangzhou Medical University; the use of these materials is approved by the Ethics Committee of these two Institutions with the permission of the patients and volunteers. Totally six patients with AML and six volunteers were recruited in this preclinical study. Mononuclear cells were isolated by Ficoll-Paque (Pharmacia, Uppsala, Sweden) density gradient. Mononuclear cell fraction was cultured in RPMI 1640 culture medium with 15% FBS.

2.3. Reagents and antibody

PtPT was synthesized in our lab. Other agents are bortezomib (BD Biosciences, San Jose, CA); NEM, Penicillin, Streptomycin, Cisplatin (Sigma–Aldrich Inc., St. Louis, MO); b-

AP15, Suc-Leu-Leu-V al-Tyr-aminomethylcoumarin (Suc-LLVY-AMC), Z-Leu-Leu-Glu-AMC (Z-LLE-AMC), Boc-Leu-Arg-Arg-AMC (Boc-LRR-AMC), 19S, 20S and 26S human proteasomes, HA-Ubiquitin-Vinyl Sulfone (HA-Ub-VS), K48-linked tetra-ubiquitin, ubiquitin-AMC (U550) (BostonBiochem, Cambridge, MA). Antibodies used in this study were purchased from following sources: anti-ubiquitin (P4D1), anti-p27 (F-8), anti-GFP (B-2) (Santa Cruz Biotechnology, Santa Cruz, CA); anti-p21 Waf1/Cip1 (DCS60), anti-caspase3 (8G10), anti-caspase8 (1C12), anti-caspase9 (C9), anti-PARP, anti-K48-linkage specific polyubiquitin (D9D5), anti-phospho-histone H2AX (Ser139) (20E3), anti-phospho-ATM (Ser1981) (D6H9), anti-phospho-Chk1 (Ser345) (133D3), anti-phospho-Chk2 (Thr68) (C13C1) (Cell Signaling Technology, Beverly, MA, USA); anti-GAPDH, anti-HA-tag (Bioworld Technology, Inc., St. Louis Park, MN, USA). Propidium iodide (PI) and Annexin V-FITC/PI apoptosis detection Kit were purchased from Keygen Company (Nanjing, China). 4,6-Diamidino-2-phenylindole (DAPI) was from Invitrogen (Guangzhou, China). Enhanced chemiluminescence (ECL) reagents were purchased from Santa Cruz Biotechnology Inc. (Santa Cruz, CA, USA).

2.4. Peptidase activity assay

Fluorogenic Suc-LLVY-AMC substrate was used to assay for chymotrypsin-like activity of the 20S proteasome [15]. To assay for *in vivo* proteasome inhibition, cancer cells were treated with PtPT or bortezomib for 4 h. The cells were lysed in ice-cold lysis buffer. Equal amounts of protein from each sample were then incubated at 37 °C with 50 μM fluorogenic substrate. To assay for direct inhibition of the 20S proteasome *in vitro*, purified human 20S proteasomes were incubated with the agent to be tested for 60 min at 37 °C before the addition of the fluorogenic substrate. Fluorescence intensity was measured using a spectrophotometer at excitation of 350 nm and emission of 438 nm (Varioskan Flash 3001, Thermo, Waltham, MA, USA).

2.5. UV absorption spectra

The UV absorption spectra of fixed amounts of DNA in Tris–HCl buffer solution were measured with addition of different concentrations of PtPT. The wavelength range of the system was from 200 to 600 nm. The blanks corresponding to the buffer were subtracted to correct the absorbance at room temperature.

2.6. Fluorescence spectra

In order to determine the optimal molar ratio of ethidium bromide (EB) to DNA, the fluorescence spectra of a fixed concentration (8.25 μM) of EB were measured with varying the concentrations of DNA from 0 to 57.75 μM. Then a 3.0 ml solution, containing a certain concentration of EB–DNA ([DNA]/[EB] = 7) complex solution, was added to a 1.0 cm quartz cuvette and titrated by successive addition of PtPT. These solutions were allowed to stand for 5 min to equilibrate. The fluorescence spectra were measured at three different temperatures (300, 305 and 310 K) in the wavelength range of 550–800 nm, with the excitation wavelength at 526 nm. The appropriate blanks corresponding to the buffer solution were subtracted to correct the background.

2.7. Cell viability assay

MTS assay (CellTiter 96Aqueous One Solution reagent; Promega, Shanghai, China) was used to test cell viability according to previously reported [40]. Briefly, 1×10^5/ml cells in 100 μl were treated with either vehicle or PtPT and other agents for 48 h. Three hours before culture termination, 20 μl MTS was added to the wells. The absorbance density was read on a 96-well plate reader at wavelength 490 nm. IC_{50} values were calculated.

2.8. Cell death assay

Apoptosis was determined by flow cytometry using Annexin V-fluoroisothiocyanate (FITC)/propidium iodide (PI) double staining. Cells were incubated with NiPT, then collected and washed with binding buffer, then incubated in working solution (100 μl binding buffer with 0.3 μl Annexin V-FITC) for 15 min in dark. Cells were washed and resuspended with binding buffer. PI was added just before flow cytometric analysis. Annexin V/PI staining was also performed as described but *in situ*. The double stained cells were also imaged with an inverted fluorescence microscope equipped with a digital camera (Axio Observer Z1, Zeiss, Germany). To monitor temporal changes in the incidence of cell death in the live culture condition, PI was added to the cell culture medium, and at the desired sequential time points, the cells in the culture dish were imaged with an inverted fluorescence microscope.

2.9. Computational modeling

To predict the binding of PtPT toward the DUBs (USP14 and UCHL5), molecular docking studies were performed with CDOCKER protocol of Discovery Studio 2.0 [Accelrys Software Inc. (2007)] as we reported previously [16]. The crystallographic structures of USP14 and UCHL5 were directly downloaded from the Protein Data Bank (PDB IDs: 2AYO and 3RIS). After removing irrelevant components, hydrogen atoms were added and their positions were minimized with a 0.01 kcal/mol/Å root mean square gradient by using the all-atom CHARMm forcefield and the Adopted Basis Newton–Raphson (NR) Algorithm. In addition, taking into account the possible hydrolysis of compound PtPT (L1) in certain physiological conditions, the hydrolysate (L2) was selected as the docking ligand. The geometry structure of compound L2 was optimized using the DFT calculations at the B3LYP/LANL2DZ level to obtain NPA charges by using the Gaussian 03 [Revision D.01, Gaussian, Inc., Wallingford, CT (2004)]. During the whole docking process, the two proteins were rigid, while the ligand L2 was flexible. The Input Site Spheres of 12 Å radius were centered on each active pocket of USP14 and UCHL5, with (x, y, z) = (38.12, 84.32, 6.61) and (−9.40, 6.57, 61.54), respectively. The conformation corresponding to the lowest CDOCKER Interaction Energy was selected as the most probable binding conformation. All parameters used in calculation were default except for those explained.

2.10. Western blot analysis

Whole cell lysates were prepared in RIPA buffer (1 × PBS, 1% NP-40, 0.5% sodium deoxycholate, 0.1% SDS) supplemented with 10 mM β-glycerophosphate, 1 mM sodium orthovanadate, 10 mM NaF, 1 mM phenylmethylsulfonyl fluoride (PMSF), and 1 × Roche Complete Mini Protease Inhibitor Cocktail (Roche, Indianapolis, IN, USA). Western blotting

was performed as previously described [17]. In brief, equal amounts of total protein extracts from cultured cells were fractionated by 12% SDS–PAGE and electrically transferred onto polyvinylidene difluoride (PVDF) membranes. Primary antibodies and appropriate horseradish peroxidase-conjugated secondary antibodies were used to detect the designated proteins. The bounded secondary antibodies on the PVDF membrane were reacted to the ECL detection reagents (Santa Cruz, CA) and exposed to X-ray films (Kodak, Rochester, NY, USA).

2.11. Nude mouse xenograft model

All animal protocols used were approved by the Institutional Animal Care and Use Committee of Guangzhou Medical University. The mice were obtained from Guangdong Laboratory Animal Monitoring Institute (SCXK2008-2002). The nude BALB/c mice (male, 18–22 g) were housed in barrier facilities with a 12 h light dark cycle, with food and water available ad *libitum*. 1–10 × 10^6 of K562 or A549 cells was inoculated subcutaneously on the flanks of 5-week-old male nude mice. After 72 h of inoculation, mice were treated with either vehicle (10% DMSO, 30% polythylene glycol 400 and 60% 0.9% NaCl) or PtPT (5 mg/kg/day) for totally 15 days (7 intervals), respectively. Tumor volumes were recorded and calculated as previously reported [18].

2.12. Immunofluorescence staining

Immunofluorescence staining was performed as reported [18]. Briefly, cell culture was performed on cover-slips in six-well plates and allowed to grow overnight. After PtPT or CDDP treatment, the cells were washed with PBS, fixed in −20 °C for 5 min with 4% paraformaldehyde, washed again in 0.2% Triton X100/PBS for 3 × 5 min and permeabilized with 1% TritonX100/PBS for 5 min. Cells were blocked with 5% bovine serum albumin (BSA)/PBS for 1 h and subsequently exposed with primary antibodies, followed by incubation with FITC-conjugated goat anti-rabbit IgG antibody (Pierce Biotechnology). Cell nuclei were counterstained with DAPI for 10 min. Samples were analyzed using a confocal laser microscope (Zeiss LSM510 Meta, Germany). All images were acquired under identical settings with LSM Image browser software.

2.13. Immunohistochemical staining

Formalin-fixed xenografts were embedded in paraffin and sectioned according to standard techniques as we previously reported [19]. Tumor xenograft sections (4 μm) were immunostained using the MaxVision kit (Maixin Biol, Fuzhou, Fujian, China) according to the manufacturer's instructions. The primary antibodies were used as indicated. Fifty microliter MaxVision™ reagent was applied to each slide. Color was developed with 0.05% diaminobenzidine and 0.03% H_2O_2 in 50 mM Tris–HCl (pH 7.6), and the slides were counterstained with hematoxylin. A negative control for every antibody was also included for each xenograft specimen by substituting the primary antibody with preimmune rabbit serum.

2.14. DUB activity assay

This was performed as reported [16]. Briefly, cell lysate (5 μg) or 26S proteasomes (25 nM) were dissolved in ice-cold DUB buffer containing 50 mM Tris–HCl (pH 7.4), 20 mM NaCl, 5 mM $MgCl_2$ and 200 μM ATP, and pretreated with PtPT or NEM for 15 min, then incubated with Ub-AMC substrate in a 100 μl reaction volume at 25 °C. Free AMC generated from substrate cleavage was temporally recorded with a microplate reader (Varioskan Flash 3001, Thermo, USA).

2.15. Ubiquitin chain disassembly

In vitro disassembly of purified polyubiquitin chains (K48-linked) was performed as described earlier. Purified 26S proteasomes (25 nM) were pre-incubated with either vehicle or PtPT for 10 min *in vitro*, and then K48-linked chains (500 ng) were added into the reaction DUB buffer for 30 min at 37 °C. The extent of chain disassembly was assessed by western blot.

2.16. Active-site-directed labeling assays

Purified 26S proteasomes (25 nM) were dissolved in DUB buffer (25 mM Tris–HCl pH 7.4, 5 mM MgCl, 20 mM NaCl, 200 μM ATP), then treated with PtPT (5, 50 μM) for 10 min before they were incubated with HA-UbVS for 1 h at 37 °C, followed by boiling in the reducing sample buffer and fractionated with SDS–PAGE. After transferring to PVDF membranes, HA-UbVS labeled DUBs were immunodetected using an HA antibody.

2.17. Detection of serum urea nitrogen (BUN) and creatinine

Blood samples were obtained by cardiac puncture on the day of euthanasia. Serum levels of blood urea nitrogen (BUN) and creatinine were measured using an automatic chemistry analyzer at the Guangzhou First Municipal People's Hospital, Guangzhou Medical University.

2.18. Statistical analysis

All the results were expressed as Mean ± SD where applicable. GraphPad Prism 4.0 software (GraphPad Software) was used for statistical analysis. Student's t test was used to compare the differences between variables. P value of <0.05 was considered statistically significant.

3. Results

3.1. PtPT dose not directly bind DNA or induce DNA damage in vitro and in vivo

First, UV absorption spectroscopy was employed to determine if PtPT binds to DNA. When compounds bind to DNA, the absorption spectroscopy shows hyperchromism (red shift) and hypochromism (blue shift), which respectively originate from the breakage of the DNA duplex secondary structure and the stabilization of the DNA duplex by either the intercalation binding or the electrostatic effect [20]. Because the intercalation involves a strong stacking interaction between an aromatic chromophore and the base pairs of DNA, the intercalation interaction is a common way of binding between compounds and DNA

[21]. The absorption spectra of PtPT with increasing concentrations of calf thymus DNA are shown in Fig. 1A; apparently no shift was found at the 300–500 nm, the characteristic absorption band of PtPT. This indicates that DNA is not changed after incubation with PtPT, suggesting that PtPT does not directly bind to DNA.

To further confirm this, we next used fluorescence spectroscopy to examine the impact of PtPT on DNA intercalation of EB. In a previous study, EB was shown to emit intense fluorescence light in the presence of DNA, due to its strong intercalation between the DNA base pairs, while the fluorescent light could be quenched by the addition of a second molecule that binds to the DNA [22]. The extent of fluorescence quenching can reflect the extent of binding between the second molecule and DNA. The fluorescence emission spectra of EB bound DNA in the absence and the presence of PtPT are given in Fig. 1B. The addition of PtPT to DNA pretreated with EB did not cause appreciable reduction in the emission intensity, indicating that there was no replacement of the EB fluorophore by PtPT and no direct binding between PtPT and the DNA.

To study whether PtPT could induce DNA damage in cultured cells, we utilized γ-H2AX as a hallmark of DNA damage response [23]. We monitored the γ-H2AX level of A549 cells treated with CDDP (2.5 μM) or PtPT (2.5 μM) using immunofluorescence. The result showed typical formation of γ-H2AX foci after treatment of CDDP but not after PtPT treatment (Fig. 1C), indicating that PtPT does not induce DNA damage in the cancer cells.

To investigate whether PtPT could interfere with the DNA damage response pathway, the dose–response and the time course of the expression of DNA damage-related proteins were detected in A549 and K562 cells. We found that CDDP strongly induced the expression of DNA damage-related proteins including γ-H2AX, p-ATM, p-chk2, and p-chk1 in both a dose- and a time-dependent manner but PtPT did not except the p-ATM in K562 cells (Fig. 1D and E). The same results were observed in non-transformed normal cells but for the p-ATM in 16HBE cells (Fig. 1F). To further test whether PtPT is a DNA damage-inducer *in vivo*, nude mice bearing A549 xenograft were injected with PtPT (5 mg/kg every day, i.p.) or CDDP (2.5 mg/kg every other day). Immunoblotting analyses showed that γ-H2AX was increased in liver and kidney tissues with CDDP treatment but not with PtPT (Fig. 1G), indicating that PtPT does not induce DNA damage in mice. Collectively, these results suggest that PtPT does not induce DNA damages.

Interestingly, we found that CdPT, a cadmium complex of pyrithione, induced the expression of DNA damage-related proteins, such as γ-H2AX, p-ATM p-chk2, and p-chk1 in cultured cells and of γ-H2AX more strongly in kidney tissue than cisplatin (Fig. 2), exhibiting a property different from PtPT.

3.2. PtPT inhibits proteasome function in cultured cancer cells

Recently we have reported that CuPT, a cooper pyrithione complex, could remarkably inhibit proteasome function [24]. To test whether PtPT is able to inhibit proteasome function as a pyrithione complex, we first measured the levels of ubiquitinated proteins in A549, A549/DDP and K562 cells incubated with PtPT, bortezomib/Velcade, CDDP, or b-AP15. As expected, PtPT induced marked increases in both total and the K48-linked ubiquitinated

proteins as well as in proteasome substrate p27 (Fig. 3A and B). Additionally, PtPT was also able to accumulate a surrogate proteasome substrate (GFPu) and total ubiquitinated proteins (Ub-prs) in a stable GFPu-HEK293 cell line (Fig. 3C and D). PtPT at 5.0 μM induced Ub-prs accumulation as strongly as Velcade at 50 nM did in these cells, and better than 0.5 μM b-AP15, a reported DUBs inhibitor (Fig. 3A). By contrast, CDDP failed to inhibit proteasome function, even at much higher doses compared with PtPT (Fig. 3A). These results suggest that PtPT can inhibit ubiquitin-mediated protein degradation. To elucidate the molecular mechanism of this action, we first tested the direct effect of PtPT on proteasome peptidase activities. We found that PtPT caused no decline of proteasome chymotrypsin-like (CT-like) activities in either purified 20S proteasomes or cultured cells, whereas Velcade substantially inhibited the proteasome activity in both assays (Fig. 4). These results suggest that PtPT does not directly block 20S proteasome peptidase activity.

3.3. PtPT inhibits the UPS by targeting DUBs USP14 and UCHL5 associated with 26S proteasomes

In general, the 26S proteasome is primarily responsible for the degradation of ubiquitinated proteins. The 26S is formed by the 20S proteasome capped by the 19S regulatory particle (RP) at one or both ends of the 20S. The proteasomal peptidase activities reside in the 20S. In the 26S proteasome, the 19S RP functions to engage ubiquitinated protein substrates, deubiquitinate the substrate, and unfold the substrate proteins before being channeled into the 20S proteolytic chamber. Given that PtPT inhibits proteasome function independently of the 20S, we hypothesized that PtPT may indirectly inhibit the proteasome via targeting the DUB activity of the 26S. The proteasome DUB activity is mainly attributed to the action of RPN11, USP14 and UCHL5 located in or associated with the 19S RP. We first assessed the effect of PtPT on the total DUB activities of cell lysates using a fluorogenic substrate Ub-AMC. Treatment with NEM (a general inhibitor of cysteine proteases) completely blocked the total DUB activities, but we did not detect any remarkable change in PtPT- or CDDP-treated groups (Fig. 5A); similarly, PtPT did not show remarkable effect on a panel of recombinant non-proteasomal DUBs (Fig. 5B). Next, we measured the DUB activity in purified 26S proteasomes co-treated with PtPT (5.0 μM). PtPT treatment exhibited complete inhibition of 26S-associated DUB activity (Fig. 5C). In addition, a dose–response test revealed that PtPT could inhibit the 26S-associated DUB activity in a dose-dependent fashion (Fig. 5D). Notably, CDDP did not show any effect on 26S-associated DUB activity (Fig. 5D). To further confirm this pharmacological action, we examined the effect of PtPT treatment on *in vitro* disassembly of purified tetraubiquitin chains (Ub4) by the 26S proteasome. K48-linked Ub chains were disassembled in the presence of 26S proteasomes and this action was attenuated by PtPT in a dose-dependent manner (Fig. 5E). These experiments demonstrate that PtPT inhibits 26S-associated DUBs selectively rather than acting broadly on all DUBs in the cell.

To identify which proteasome-associated DUBs can be inhibited by PtPT, we first performed computational docking study to predict the binding information between PtPT and 26S-associated DUBs including USP14 and UCHL5. The chemical structures of PtPT (L1) and its metabolized product (L2), a hydrolysate of PtPT, are shown in Fig. 5F. Previous studies revealed that the catalytic core in the active site of USP14 is formed by Cys113, His434 and

Asp450 [25], and that of UCHL5 is formed by Cys88, His164 and Asp179 [26]. The docking analyses predict that PtPT could bind to the active sites of USP14 and UCHL5, with CDOCKER Interaction Energy of −15.99 and −16.78 kcal mol^{-1}, and the binding modes are dis-played in Fig. 5F. In the binding site of USP14, the S atom of Cys113 coordinates to Pt^{2+} with distances of 2.939 Å. In addition, one hydrogen bond of 2.483 Å is formed between the polar H of Cys113 and the O atom of PtPT. In the binding site of UCHL5, there are two coordination bonds between the Pt^{2+} and two side chains, His164 and Phe165, with corresponding bond lengths of 3.350 and 2.550 Å. At the same time, the S atom of PtPT forms two hydrogen bonds with Cys88 and Gln91 (2.140 and 1.194 Å). These calculation results suggest that PtPT can bind to the catalytic cores of USP14 and UCHL5 through coordination bonds and hydrogen bonds. To confirm the computational docking results, we performed competitive labeling experiments using HA tagged ubiquitin vinylsulphonone (HA-UbVS), an active site probe of cysteine DUBs. Incubation of PtPT with 26S proteasomes abolished UbVS binding with either UCHL5 or USP14 in a dose-dependent manner (Fig. 5G). These computational and experimental results indicate that PtPT can selectively target UCHL5 and USP14, two proteasome-associated DUBs.

3.4. PtPT induces cytotoxicity in cultured cancer cells

Previous reports have shown up-regulation of proteasome activities in many different types of cancers, such as colon and prostate cancers as well as leukemia [27–29], suggesting that cancer cells may depend more upon the UPS for survival and growth than non-cancer cells. Therefore, we examined whether inhibition of 26S-associated DUBs via PtPT treatment would selectively induce cytotoxicity in a panel of cancer cells (K562, U266, A549, SMMC-7721, A549/DDP). These experiments also included cisplatin (CDDP) for comparison. We first investigated the effect of PtPT and CDDP on these cultured cells using MTS assay, our results indicated that exposure to increasing doses of PtPT over a period of 48 h decreased the viability of these cancer cells in a dose-dependent fashion and showed better efficacy than CDDP, except for cisplatin-sensitive cells A549 to which PtPT and CDDP showed comparable efficacy (Fig. 6A–E). Importantly, we found that PtPT could partially overcome the CDDP resistance of A549/DDP cells (Fig. 6C). It was important to note that viability inhibition of PtPT at a dose up to 5 μM toward non-transformed normal cells (e.g., LO2, 16HBE) (Fig. 6F and G) was much less than that toward cancer cells; however, this selective inhibition was not observed from cisplatin. We next analyzed the capacity of PtPT to induce cell death in cisplatin-sensitive cell line. A549 cells were exposed to PtPT for either 24 or 36 h, followed by recording the PI (propidium iodide)-positive cells with fluorescence microscopy. We observed that PtPT induced a dose-dependent cell death started as early as 24 h while CDDP did not induce marked cell death until 36 h (Fig. 6H). Furthermore, PtPT-induced apoptosis is shown in Fig. 6I and J. A549 and K562 cells were treated with the indicated dose of PtPT and CDDP for 24 h, apoptotic cells were detected by flow cytometry with Annexin V/PI staining. The results revealed that PtPT could dose-dependently induce cell apoptosis more effectively than CDDP. Taken together, these findings suggest that the selectivity profile and effectiveness of PtPT to kill cancer cells *in vitro* are better than those of CDDP which is currently licensed for clinical use.

3.5. PtPT-induced apoptosis is associated with caspase activation

To test whether the cytotoxicity of lung adenocarcinoma cancer cell lines following PtPT treatment is associated with caspase activation, the amplitude of mitochondrial membrane potential (MMP) disruption was assessed after PtPT treatment by flow cytometry in A549 and A549/DDP cells. The data showed that PtPT induced a dose-dependent loss of MMP in the cells (Fig. 7A), suggesting that an apoptosis-inducing mechanism is triggered by PtPT treatment. Fig. 7B shows the dose-dependent release of cytochrome c and AIF from mitochondria into cytosol after being exposed to PtPT for 12 h. To further investigate the mechanism of PtPT-induced apoptosis, the activation of the caspase cascade was investigated. A549 and A549/DDP were incubated with PtPT, followed by western blot analysis. The results showed that the induction of cleaved PARP by PtPT treatment paralleled the increase of the active forms of caspases-3 in a dose- and time-dependent pattern, and the cleavage of procaspase-9 was induced concomitantly with that of procaspase-3, −8 in a similar pattern to PARP cleavage (Fig. 7C). Collectively, these results indicate that PtPT triggers lung adenocarcinoma cancer cell apoptosis via caspase activation.

3.6. Proteasome inhibition is required for PtPT to induce apoptosis

If inhibition of the proteasome is responsible for induction of apoptosis, inhibition of proteasome should occur prior to cell death. To test this hypothesis, we determined the time course of PtPT-induced proteasome inhibition. A549, A549/DDP and K562 cells were treated with either vehicle or 2.5 μM of PtPT for 6, 12, 18, 24 h, followed by detection of total, K48-linked ubiquitinated proteins and proteasome substrate p27 using western blot analyses. We found that accumulation of ubiquitinated proteins was observed during the course of treatment as early as 6 h (Fig. 8A and B). Accumulation of p27 was also found to be time dependent. Importantly, apoptosis-specific PARP cleavage was not observed until 12 h of PtPT treatment (Fig. 8A and B). These results show that the apoptosis induced by PtPT occurs after the proteasome inhibition. Next, we tested the effect of EDTA (ethylenediaminetetraacetic acid), a chelating agent for metal ions such as Pt^{2+}, on the PtPT induction of proteasome inhibition and cell death. Fig. 8C shows that PtPT exhibited diminished reactivity after being bound by EDTA. As expected, EDTA partially reversed PtPT-induced ubiquitinated protein accumulation; and PARP cleavage (indicators of apoptosis) was accordingly abolished in A549 cells (Fig. 8D). This diminished effect on cell death was also confirmed using propidium (PI) staining followed by inverted fluores-cent microscopy (Fig. 8E). Therefore, proteasome inhibition is required for apoptosis induction by PtPT.

3.7. PtPT specifically induces cytotoxicity and proteasome inhibition in cancer cells from leukemia patients

To further evaluate the antineoplastic effects of PtPT, bone marrow cells from six leukemia patients were treated *ex vivo* with increasing doses of PtPT. Peripheral blood mononuclear cells (PBMCs) from 6 healthy volunteers were used as controls. We found that the average IC50 values for PtPT in normal PBMCs were about 4.413 ± 0.392 μM, approximately 6 times higher than that for primary monocytes obtained from leukemia patients (0.754 ± 0.102 μM) (Fig. 9A). In contrast, the IC50 values of cisplatin for the two types of cells

were similar; and importantly, the IC50 of cisplatin for leukemia cells was much higher than that of PtPT (Fig. 9B). Additionally, the difference in the IC50 values of bortezomib toward the normal and leukemia monocytes was not as dramatic as those of PtPT (Fig. 9C). PtPT treatment for 24 h at doses ranging from 0.25 to 1.0 μM resulted in significant apoptosis in the monocytes from leukemia patients as detected with Annexin V/PI staining by flow cytometry (Fig. 9D) or by fluorescence microscope (Fig. 9E). Treatment with PtPT significantly increased the level of Ub-prs and cleaved PARP in cancer cells from AML patients (Fig. 9F). In contrast, CDDP failed to induce marked cell death and accumulation of Ub-prs even at a dose as high as 10 μM (Fig. 9E and F). Nonetheless, PtPT treatment at 5 μM started to cause detectable cell death in monocytes from healthy volunteers (Fig. 9G). These results clearly demonstrate that PtPT specifically induces *ex vivo* proteasome inhibition and cytotoxicity in primary human cancer cells.

3.8. PtPT inhibits proteasome function and tumor growth in vivo

We next evaluated the effect of PtPT on tumor growth *in vivo* using nude mouse xenograft models. PtPT was administered to BALB/c nude mice bearing A549 and K562 xenografts, the tumor size curves and images showed a significant reduction of tumor burden in mice treated with PtPT versus the control group (Fig. 10A and B, J and K). Consistent with the reduction in tumor growth, PtPT-treated mice also showed a reduction in tumor weight (Fig. 10C and L). Importantly, we observed no change in mouse behavior or loss in body weight (Fig. 10D and M). In the A549 xenograft model, we used CDDP as a positive control. In the CDDP-treated group, it was found that CDDP exhibited more effective antitumor activity but an obvious reduction of body weight was also detected (Fig. 10D). We also test the content of AST and ALT (two indicators of liver function) in mouse serum. We found that CDDP treatment induced dramatic increases of these two enzymes in the serum but PtPT did not (Fig. 10E). To assess nephrotoxicity in mouse treated with PtPT, we compared the acute kidney injury (AKI) of PtPT and CDDP by intraperitoneal (ip) injection of a single dose of 15 mg/kg respectively in nude mice, and found that CDDP-treated group showed significant renal impairment, as indicated by significantly increased levels of serum urea nitrogen (BUN) and creatinine as well as marked histologic damage in animals at day 4 after CDDP application (Fig. 10F–H). Conversely, there were not any detectable changes in either biochemical or histologic indicators of AKI in the PtPT-treated group (Fig. 1F–H). The immunostaining analysis was performed to detect the effect of PtPT on *in vivo* proteasome function. The results showed that highly increased levels of proteasome substrates including total and K48-linked ubiquitinated proteins were observed in the PtPT-treated tumor tissues, accompanied by caspase-3 activation (Fig. 10I and N). Hence, in contrast to CDDP, PtPT could selectively inhibit *in vivo* tumor growth without apparent non-specific toxicity, with a distinct mechanism involving proteasome inhibition.

4. Discussion

By targeting DNA, platinum-based drugs, as exemplified by cisplatin, are a giant pillar in current clinical cancer chemotherapy; however, the adverse effects and drug resistance that are inherent to the DNA targeting by this drug family are major problems limiting their clinical use and efficacy. Hence, search for more tolerable and effective alternatives for

cisplatin is imperative. To this end, the present study represents a very exciting breakthrough because we have identified a new platinum-based anti-cancer agent (PtPT) which operates via selective inhibition of proteasomal DUBs rather than indiscriminately targeting DNA. This target switch endows PtPT with remarkably improved selectivity and greater potency in killing cancers both *in vitro* and *ex vivo*, and with a much more favorable safety profile than cisplatin as revealed by the preclinical *in vivo* trial using a tumor xenograft mouse model.

Chemical complexes containing metal ions, such as gallium (III), copper (II), zinc (II), nickel (II), and cobalt (II), were designed to target the 26S proteasome in the past decade [30–33]. The discovery that these metal-based complexes exert their antiproliferative action by suppressing proteasomal proteolytic peptidase activities provided a potentially new direction in developing new cancer therapy. Although several essential or nonessential metals have been reported to interfere with UPS function, platinum, a pioneer of metal medication, has long been confined to the DNA cage. The present study unveils for the first time that by complexing with pyrithione, platinum no longer binds to DNA but targets effectively the 26S proteasome-associated DUBs instead. This is compellingly supported by a preponderance of *in vitro* and *in vivo* evidence (Figs. 1–3). Previous work has shown that the platinum center of cisplatin reacts with DNA, forming two covalent bonds to N7 atoms of two adjacent guanine bases. Here our *in vitro* tests demonstrate that, unlike cisplatin, PtPT does not bind DNA with a typical inter-calative binding or covalent interaction. This has also been shown by Vieites et al. using agarose gel electrophoresis [34]. Furthermore, our results obtained from immunofluorescence and western blot analyses using γ-H2AX as an indicator of DNA damage in cultured cells and mice are in agreement with our conclusion dawn from *in vitro* findings. Indeed no increased levels of DNA damage markers such as p-ATM or γ-H2AX were induced by PtPT treatment, suggesting that PtPT is non-genotoxic; this is starkly different from cisplatin. Through induction of DNA damage or genotoxic stress, cisplatin led to a rapid activation of ATM and then phosphorylates Chk1 and Chk2 and H2AX in tumor cells. We also observed increased expression of γ-H2AX in the kidney and liver tissues of cisplatin-, but not PtPT-, treated mice. This is of vital importance because DNA damage in renal cells and tissues causes cisplatin nephrotoxicity [35]. Moreover, we show that CdPT, a cadmium complex of pyrithione, induces DNA damage response similarly to cisplatin *in vitro* and more strongly in kidney than cisplatin, exhibiting a property vastly different from PtPT. These results indicate that the platinum metal ion is an important determinant of the observed effects from PtPT. Notably, PtPT is also highly effective in inducing cytotoxicity in cisplatin-resistant cells, which is not only consistent with the notion that PtPT does not act on DNA damage-based biotargets but also suggests that PtPT can be a promising drug candidate for overcoming cisplatin-resistance.

We also have provided multiple lines of evidence that PtPT takes a mechanism distinct from the classical proteasome inhibitor bortezomib to accumulate endogenous and surrogate proteasome substrates. The extent of proteasome inhibition induced by PtPT is comparable to bortezomib as reflected by their similar effects on accumulation of both Ub-prs and GFPu. However, analyses of computational docking and enzyme inhibition show that PtPT displays properties consistent with a mechanism of competitive inhibition of 26S proteasome DUB activity. Recently, a series of compounds including WP1130, AC17, b-AP15, and b-AP15-derivative analogs (e.g., RA-9, VLX1570), which all contain α, β

unsaturated dienones (i.e., Michael acceptors), were reported to inhibit proteasome DUBs [36–40]. All of these DUB inhibitors are electrophiles and would be expected to confer nonspecific reactivity. Indeed, it was found that RA-9 inhibited *in vitro* UCHL1, UCHL3, USP8 and USP9x, besides USP14 and UCHL5. WP1130 was also found to inhibit a broader spectrum of DUBs. In our docking for the bound PtPT models, we find the formation of coordination and hydrogen bonds between Pt^{2+} and the specific amino acid residue of USP14 and UCHL5, a reaction model distinct from Michael reaction of α, β unsaturated dienones. This is experimentally confirmed by our comparison of the ability of PtPT to inhibit the proteasomal and non-proteasomal DUBs. PtPT did not show discernible effect on either overall cellular DUB activities or a panel of recombinant non-proteasomal DUBs but remarkably inhibited 26S proteasome-associated DUB activity in a dose-dependent manner. PtPT is also distinct from CuPT, a metal complex reported in our previous work [24], which acts as both a broad-spectrum DUB inhibitor and 20S proteasome peptidase inhibitor, inducing highly toxic effects *in vitro*, *in situ* and *in vivo*. Collectively, these results demonstrate that only PtPT but not other metal pyrithione compounds tested so far (copper, cadmium) exerts proteasome inhibition by selectively targeting proteasomal UCHL5 and USP14. PtPT is also strikingly distinct from IU1, a USP14 inhibitor reported previously [41], which inhibits USP14 but not UCHL5 activity and promotes the degradation of ubiquitinated proteins.

In summary, unlike cisplatin which targets DNA, PtPT targets primarily proteasomal DUBs instead of DNA and exhibits better anticancer effects than cisplatin (Fig. 11). The DNA-platination of clinical Pt-based drugs rests in the coordination around the metal ion of two non-leaving groups (N–Pt bonds) and of two fast-rate leaving groups (i.e., chlorides). The rate of DNA-platination is modulated by the nature of the leaving groups. The presence of two medium-rate leaving groups (i.e., pyrithione containing S and O atom) allows them to react with protein targets even before PtPT reaches the nucleus. Hence, the ligand pyrithione endows platinum with the capacity to selectively target proteasomal DUBs.

Others have shown that cancer cells possess progressive up-regulation of the metabolic machinery to sustain the increased proliferation rate [42–44]. This phenomenon renders cancer cells more sensitive to UPS inhibition. In this study, we showed that inhibition of proteasome-associated DUBs by PtPT treatment selectively suppressed the cell viability of multiple types of cancer cells in cultures. Importantly, PtPT treatment caused marked reduction in cell viability of A549 cells and their cisplatin-resistant parental lines. Notably, PtPT selectively induced Ub-prs accumulation and apoptosis in primary cancer cells from leukemia patients but much less cell death in normal mononuclear cells than in cancer cells. On the contrary, cisplatin as a genotoxic agent induces cytotoxicity in normal cells similarly to the cancer cells. In addition to our *in vitro* studies, we also examined anticancer activity of PtPT *in vivo*. Our results showed that treatment of cancer xenografts with PtPT significantly retarded tumor growth. Importantly, compared with cisplatin, PtPT treatment was not associated with toxicity, including reduction of body weight and liver function and perturbed renal histology and function that are commonly seen in CDDP treatment. These results strongly suggest that PtPT is a better anticancer candidate than cisplatin and could be used in the treatment of multiple cancers. As expected, the chymotrypsin-like activity of tumor tissues was not inhibited with PtPT treatment (data not shown), while bortezomib could

inhibit chymotrypsin-like activity in tumor or other tissues as we previously reported [45], further confirming that PtPT inhibits the UPS *in vivo* via targeting proteasomal DUBs.

Even though we could not completely exclude other binding partners of PtPT, our *in vitro* and *in vivo* findings demonstrate that targeting the proteasomal DUBs UCHL5 and USP14 is a major mechanism for the selective anticancer activity of PtPT.

Acknowledgements

We thank Xiuhua Liu, the College of Chemistry and Chemical Engineering of Henan University for DNA binding detection. We also thank the Guangdong Provincial Key Laboratory of Malignant Tumor Epigenetics and Gene Regulation, Sun Yat-Sen Memorial Hospital, Sun Yat-Sen University for flow cytometry detection.

Funding

This work was supported by the National High Technology Research and Development Program of China (2006AA02Z4B5); NSFC (81272451/H1609, 81472762/H1609); Key Projects (10A057S) from Guangzhou Education Commission and a project (2010A060801016) from Guangdong Key Laboratory of Urology (to J.L.); NSFC (81201719/H1609) (to H.H.) and in part by US NIH grants HL072166 and HL085629 (to X.W.).

References

[1]. Hsu DS, Balakumaran BS, Acharya CR, Vlahovic V, Walters KS, Garman K, et al. Pharmacogenomic strategies provide a rational approach to the treatment of cisplatin-resistant patients with advanced cancer. J. Clin. Oncol. 2007; 25:4350–4357. [PubMed: 17906199]

[2]. Rabik CA, Dolan ME. Molecular mechanisms of resistance and toxicity associated with platinating agents. Cancer Treat. Rev. 2007; 33:9–23. [PubMed: 17084534]

[3]. Jamieson ER, Lippard SJ. Structure, recognition, and processing of cisplatin-DNA adducts. Chem. Rev. 1999; 99:2467–2498. [PubMed: 11749487]

[4]. Raymond E, Faivre S, Chaney S, Woynarowski J, Cvitkovic E. Cellular and molecular pharmacology of oxaliplatin. Mol. Cancer Ther. 2002; 1:227–235. [PubMed: 12467217]

[5]. Richardson PG, Barlogie B, Berenson J, Singhal S, Jagannath S, Irwin D, et al. A phase 2 study of bortezomib in relapsed, refractory myeloma. New Engl. J. Med. 2003; 348:2609–2617. [PubMed: 12826635]

[6]. Adams J. The proteasome: structure, function, and role in the cell. Cancer Treat. Rev. 2003; 29(Suppl. 1):3–9.

[7]. Komander D, Clague MJ, Urbe S. Breaking the chains: structure and function of the deubiquitinases. Nat. Rev. Mol. Cell Biol. 2009; 10:550–563. [PubMed: 19626045]

[8]. Fraile JM, Quesada V, Rodriguez D, Freije JM, Lopez-Otin C. Deubiquitinases in cancer: new functions and therapeutic options. Oncogene. 2012; 31:2373–2388. [PubMed: 21996736]

[9]. Hussain S, Zhang Y, Galardy PJ. DUBs and cancer: the role of deubiquitinating enzymes as oncogenes, non-oncogenes and tumor suppressors. Cell Cycle. 2009; 8:1688–1697. [PubMed: 19448430]

[10]. Peth A, Kukushkin N, Bosse M, Goldberg AL. Ubiquitinated proteins activate the proteasomal ATPases by binding to Usp14 or Uch37 homologs. J. Biol. Chem. 2013; 288:7781–7790. [PubMed: 23341450]

[11]. Finley D. Recognition and processing of ubiquitin-protein conjugates by the proteasome. Annu. Rev. Biochem. 2009; 78:477–513. [PubMed: 19489727]

[12]. D'Arcy P, Linder S. Molecular pathways: translational potential of deubiquitinases as drug targets. Clin. Cancer Res. 2014; 20:3908–3914. [PubMed: 25085788]

[13]. Bence NF, Sampat RM, Kopito RR. Impairment of the ubiquitin-proteasome system by protein aggregation. Science. 2001; 292:1552–1555. [PubMed: 11375494]

[14]. Huang H, Zhang X, Li S, Liu N, Lian W, McDowell E, et al. Physiological levels of ATP negatively regulate proteasome function. Cell Res. 2010; 20:1372–1385. [PubMed: 20805844]

[15]. Yang H, Zhou P, Huang H, Chen D, Ma N, Cui QC, et al. Shikonin exerts antitumor activity via proteasome inhibition and cell death induction in vitro and in vivo. Int. J. Cancer. 2009; 124:2450–2459. [PubMed: 19165859]

[16]. Liu N, Li X, Huang H, Zhao C, Liao S, Yang C, et al. Clinically used antirheumatic agent auranofin is a proteasomal deubiquitinase inhibitor and inhibits tumor growth. Oncotarget. 2014; 5:5453–5471. [PubMed: 24977961]

[17]. Huang H, Liu N, Guo H, Liao S, Li X, Yang C, et al. L-carnitine is an endogenous HDAC inhibitor selectively inhibiting cancer cell growth in vivo and in vitro. PLoS One. 2012; 7:e49062. [PubMed: 23139833]

[18]. Shi X, Chen X, Li X, Lan X, Zhao C, Liu S, et al. Gambogic acid induces apoptosis in imatinib-resistant chronic myeloid leukemia cells via inducing proteasome inhibition and caspase-dependent Bcr-Abl downregulation. Clin. Cancer Res. 2014; 20:151–163. [PubMed: 24334603]

[19]. Lu L, Qin A, Huang H, Zhou P, Zhang C, Liu N, et al. Shikonin extracted from medicinal Chinese herbs exerts anti-inflammatory effect via proteasome inhibition. Eur. J. Pharmacol. 2011; 658:242–247. [PubMed: 21392503]

[20]. Zhong W, Yu JS, Huang W, Ni K, Liang Y. Spectroscopic studies of interaction of chlorobenzylidine with DNA. Biopolymers. 2001; 62:315–323. [PubMed: 11857270]

[21]. Kashanian S, Khodaei MM, Pakravan P. Spectroscopic studies on the interaction of isatin with calf thymus DNA. DNA Cell Biol. 2010; 29:639–646. [PubMed: 20590475]

[22]. Jiang CQ, He JX, Wang JS. [Studies on the interaction mode between polymyxin B sulfate and DNA with EB as a fluorescence probe]. Guang pu xue yu guang pu fen xi = Guang pu. 2002; 22:103–106. [PubMed: 12940041]

[23]. Redon CE, Dickey JS, Bonner WM, Sedelnikova OA. Gamma-H2AX as a biomarker of DNA damage induced by ionizing radiation in human peripheral blood lymphocytes and artificial skin. Adv Space Res. 2009; 43:1171–1178. [PubMed: 20046946]

[24]. Liu N, Liu C, Li X, Liao S, Song W, Yang C, et al. A novel proteasome inhibitor suppresses tumor growth via targeting both 19S proteasome deubiquitinases and 20S proteolytic peptidases. Sci. Rep. 2014; 4:5240. [PubMed: 24912524]

[25]. Hu M, Li P, Song L, Jeffrey PD, Chenova TA, Wilkinson KD, et al. Structure and mechanisms of the proteasome-associated deubiquitinating enzyme USP14. EMBO J. 2005; 24:3747–3756. [PubMed: 16211010]

[26]. Maiti TK, Permaul M, Boudreaux DA, Mahanic C, Mauney S, Das C. Crystal structure of the catalytic domain of UCHL5, a proteasome-associated human deubiquitinating enzyme, reveals an unproductive form of the enzyme. FEBS J. 2011; 278:4917–4926. [PubMed: 21995438]

[27]. Lee K, Kang JE, Park SK, Jin Y, Chung KS, Kim HM, et al. LW6, a novel HIF-1 inhibitor, promotes proteasomal degradation of HIF-1alpha via upregulation of VHL in a colon cancer cell line. Biochem. Pharmacol. 2010; 80:982–989. [PubMed: 20599784]

[28]. Rico-Bautista E, Yang CC, Lu L, Roth GP, Wolf DA. Chemical genetics approach to restoring p27Kip1 reveals novel compounds with antiproliferative activity in prostate cancer cells. BMC Biol. 2010; 8:153. [PubMed: 21182779]

[29]. Niewerth D, Jansen G, Riethoff LF, van Meerloo J, Kale AJ, Moore BS, et al. Antileukemic activity and mechanism of drug resistance to the marine Salinispora tropica proteasome inhibitor salinosporamide A (Marizomib). Mol. Pharmacol. 2014; 86:12–19. [PubMed: 24737138]

[30]. Chen D, Cui QC, Yang H, Dou QP. Disulfiram, a clinically used anti-alcoholism drug and copper-binding agent, induces apoptotic cell death in breast cancer cultures and xenografts via inhibition of the proteasome activity. Cancer Res. 2006; 66:10425–10433. [PubMed: 17079463]

[31]. Chen D, Cui QC, Yang H, Barrea RA, Sarkar FH, Sheng S, et al. Clioquinol, a therapeutic agent for Alzheimer's disease, has proteasome-inhibitory, androgen receptor-suppressing, apoptosis-inducing, and antitumor activities in human prostate cancer cells and xenografts. Cancer Res. 2007; 67:1636–1644. [PubMed: 17308104]

[32]. Cvek B, Milacic V, Taraba J, Dou QP. Ni(II), Cu(II), and Zn(II) diethyldithiocarbamate complexes show various activities against the proteasome in breast cancer cells. J. Med. Chem. 2008; 51:6256–6258. [PubMed: 18816109]

[33]. Tomco D, Schmitt S, Ksebati B, Heeg MJ, Dou QP, Verani CN. Effects of tethered ligands and of metal oxidation state on the interactions of cobalt complexes with the 26S proteasome. J. Inorg. Biochem. 2011; 105:1759–1766. [PubMed: 22056177]

[34]. Vieites M, Smircich P, Parajon-Costa B, Rodriguez J, Galaz V, Olea-Azar C, et al. Potent in vitro anti-Trypanosoma cruzi activity of pyridine-2-thiol N-oxide metal complexes having an inhibitory effect on parasite-specific fumarate reductase. J. Biol. Inorg. Chem. 2008; 13:723–735. [PubMed: 18322709]

[35]. Pabla N, Huang S, Mi QS, Daniel R, Dong Z. ATR-Chk2 signaling in p53 activation and DNA damage response during cisplatin-induced apoptosis. J. Biol. Chem. 2008; 283:6572–6583. [PubMed: 18162465]

[36]. Kapuria V, Peterson LF, Fang D, Bornmann WG, Talpaz M, Donato NJ. Deubiquitinase inhibition by small-molecule WP1130 triggers aggresome formation and tumor cell apoptosis. Cancer Res. 2010; 70:9265–9276. [PubMed: 21045142]

[37]. D'Arcy P, Brnjic S, Olofsson MH, Fryknas M, Lindsten K, De Cesare M, et al. Inhibition of proteasome deubiquitinating activity as a new cancer therapy. Nat. Med. 2011; 17:1636–1640. [PubMed: 22057347]

[38]. Zhou B, Zuo Y, Li B, Wang H, Liu H, Wang X, et al. Deubiquitinase inhibition of 19S regulatory particles by 4-arylidene curcumin analog AC17 causes NF-kappaB inhibition and p53 reactivation in human lung cancer cells. Mol. Cancer Ther. 2013; 12:1381–1392. [PubMed: 23696216]

[39]. Coughlin K, Anchoori R, Iizuka Y, Meints J, MacNeill L, Vogel RI, et al. Small-molecule RA-9 inhibits proteasome-associated DUBs and ovarian cancer in vitro and in vivo via exacerbating unfolded protein responses. Clin. Cancer Res. 2014; 20:3174–3186. [PubMed: 24727327]

[40]. Wang X, D'Arcy P, Caulfield TR, Paulus A, Chitta K, Mohanty C, et al. Synthesis and evaluation of derivatives of the proteasome deubiquitinase inhibitor b-AP15. Chem. Biol. Drug. Des. 2015

[41]. Lee BH, Lee MJ, Park S, Oh DC, Elsasser S, Chen PC, et al. Enhancement of proteasome activity by a small-molecule inhibitor of USP14. Nature. 2010; 467:179–184. [PubMed: 20829789]

[42]. Bazzaro M, Lee MK, Zoso A, Stirling WL, Santillan A, Shih Ie M, et al. Ubiquitin-proteasome system stress sensitizes ovarian cancer to proteasome inhibitor-induced apoptosis. Cancer Res. 2006; 66:3754–3763. [PubMed: 16585202]

[43]. Bazzaro M, Lin Z, Santillan A, Lee MK, Wang MC, Chan KC, et al. Ubiquitin proteasome system stress underlies synergistic killing of ovarian cancer cells by bortezomib and a novel HDAC6 inhibitor. Clin. Cancer Res. 2008; 14:7340–7347. [PubMed: 19010849]

[44]. Raj L, Ide T, Gurkar AU, Foley M, Schenone M, Li X, et al. Selective killing of cancer cells by a small molecule targeting the stress response to ROS. Nature. 2011; 475:231–234. [PubMed: 21753854]

[45]. Li X, Liu S, Huang H, Liu N, Zhao C, Liao S, et al. Gambogic acid is a tissue-specific proteasome inhibitor in vitro and in vivo. Cell Rep. 2013; 3:211–222. [PubMed: 23260670]

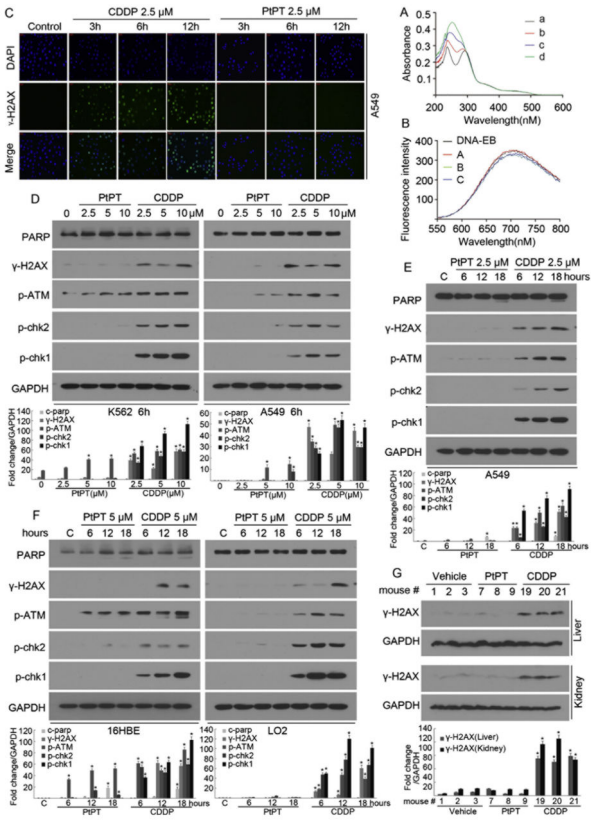

Fig. 1.

PtPT dose not induce DNA damage *in vitro* and *in vivo*. (A) UV absorption spectra of PtPT (8.96×10^{-6} M) with various concentrations of DNA [0 (a), 1.42 (b), 2.85 (c), 4.27 (d) × 10^{-5} M]. (B) Fluorescence spectra of DNA-EB with various concentrations of PtPT. c(EB) = 2 μM; c(DNA) = 1.4×10^{-5} M, c(PtPT) = [1.2 (A), 3.1 (B), 6.4 (C) × 10^{-5} M]. (C) Immunostaining of γ-H2AX at different times after exposure to CDDP or PtPT. A549 cells were treated with CDDP (2.5 μM) or PtPT (2.5 μM) for indicated times, followed by immunofluorescence staining assay. Green: γ-H2AX, blue: nuclei stained with DAPI (scale bar, 50 μm). (D–F) DNA damage-related protein expression. Cancer cells (A549/K562) and non-transformed normal cells (16HBE/LO2) were incubated with PtPT or CDDP to detect dose- and time-dependent effects. DNA damage-related proteins including γ-H2AX, p-ATM, p-chk2, p-chk1 and PARP were detected by western blot. (G) DNA damage response in mouse tissue. Nude mice bearing A549 xenograft were injected with PtPT (5 mg/kg/day, i.p.) or CDDP (2.5 mg/kg/2 day), liver and kidney tissues were collected for western blots for γ-H2AX. One representative blot (D/E/F/G, upper panel) out of three independent experiments is shown and quantified by densitometric analysis (lower panel). Values are expressed as mean ± SD ($n = 3$). $^{*}P < 0.05$, compared with each control.

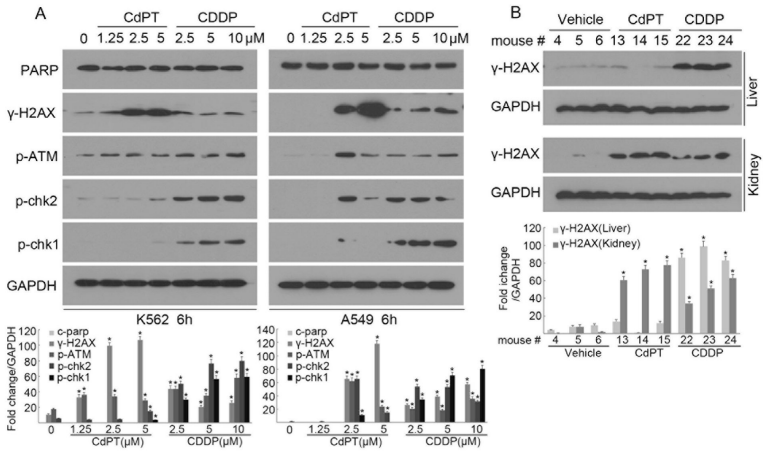

Fig. 2.

CdPT induces DNA damage *in vitro* and *in vivo*. (A) CdPT induces DNA damage responses. Cancer cells (A549/K562) were incubated with various doses of CdPT or CDDP, DNA damage-related proteins including γ-H2AX, p-ATM, p-chk2, p-chk1 and PARP were analyzed by western blot. (B) DNA damage in mouse tissues. Nude mice bearing A549 xenograft were i.p. injected with CdPT (5 mg/kg/2 day) or CDDP (2.5 mg/kg/day), liver and kidney tissues were collected for western blots for γ-H2AX. One representative blot (A/B, upper panel) out of three independent experiments is shown and quantified by densitometric analysis (lower panel). Values are expressed as mean ± SD ($n = 3$). $^{*}P < 0.05$, compared with each control.

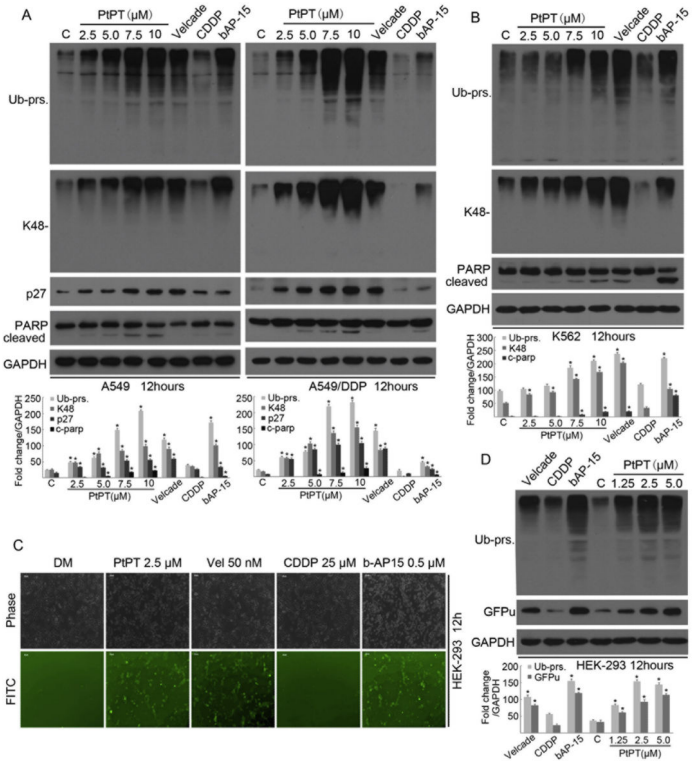

Fig. 3.

PtPT inhibits proteasome function in multiple cancer cells. (A and B) Dose-dependent accumulation of proteasomal substrates in K562, A549 and A549/DDP cells. These cells were treated with PtPT (2.5, 5, 7.5, 10 μM), bortezomib/Velcade (Vel, 50 nM), CDDP (20 μM), or b-AP15 (0.5 μM) for 12 h, followed by detecting the levels of total (Ub-prs) and K48-linked (K48-) ubiquitin conjugates, p27, and PARP cleavage with western blot analysis. (C and D) The changes of a surrogate proteasome substrate (GFPu). HEK-293 cells stably expressing GFPu were treated with PtPT for 12 h, then ubiquitinated proteins and GFPu protein were detected with western blot or imaged under an inverted fluorescence microscope (scale bar, 50 μm). Bortezomib/Velcade (Vel) and b-AP15 were used as positive controls. CDDP was used as a negative control. One representative blot (A/B/D, upper panel) out of three independent experiments is shown and quantified by densitometric analysis (lower panel). Values are expressed as mean ± SD ($n = 3$). $^{*}P < 0.05$, compared with each control.

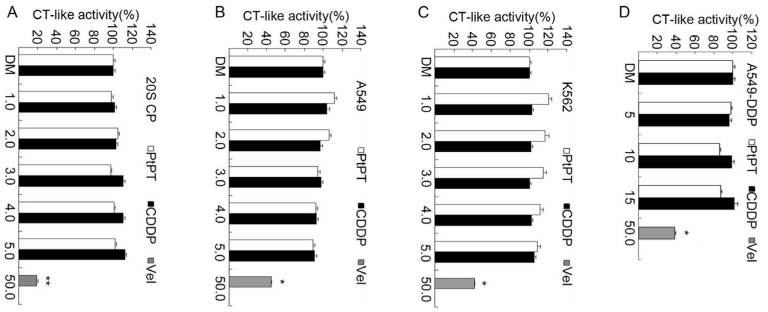

Fig. 4.

PtPT does not inhibit 20S proteasome peptidase activities *in vitro*. (A) The effect of PtPT on 20S proteasome peptidase activities *in vitro*. 20S proteasomes were treated with different doses of PtPT or CDDP; and Chymotrypin-like activity was measured using specific synthetic fluorogenic substrate. Bortezomib/Velcade (Vel) was used as a positive control. (B–D) The *in situ* effect of PtPT on proteasome peptidase activity. K562 (B), A549 (C) and A549/DDP (D) cells were treated with increasing doses of PtPT or CDDP for 6 h, and Chymotrypsin-like activity was assayed. Bortezomib/Velcade (Vel) was used as a positive control. $n = 3$, mean ± SD. $^{*}P < 0.05$, compared with each control.

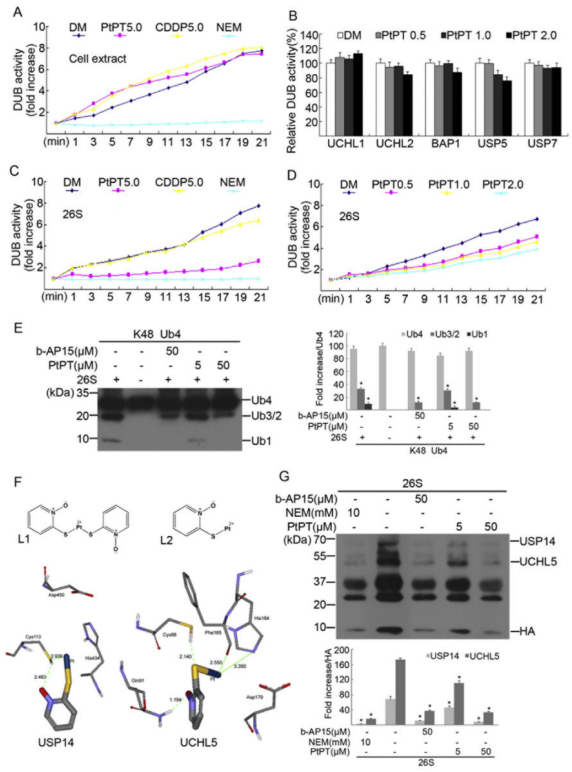

Fig. 5.

PtPT inhibits proteasomal deubiquitinase (DUB) USP14 and UCHL5. (A) The effect of PtPT on cytoplasmic total DUB activities. A549 cell lysates were exposed to PtPT (5.0 μM) and dynamic DUB activity was measured. NEM was used as a positive control. (B) The effect of PtPT at the indicated dosages on the activity of 5 recombinant non-proteasomal deubiquitinases (UCHL1, UCHL2, BAP1, USP5, and USP7) was tested. End-point DUB activity is shown. $n = 3$, Mean ± SD. (C) The effect of PtPT on proteasomal DUB activities. Purified 26S proteasomes were incubated with PtPT or CDDP (5.0 μM), and then DUB activity kinetics were measured. NEM was used as a positive control. (D) Purified 26S proteasomes were treated with PtPT (0.5, 1.0, 2.0 μM), then dynamic DUB activity was recorded. (E) Ubiquitin chain disassembly assay. The disassembly of K48-linked ubiquitin tetramers mediated by the 26S proteasome was detected in the presence of PtPT or b-AP15.One representative blot (E/left panel) out of three independent experiments is shown and quantified by densitometric analysis (E/right panel). Values are expressed as mean ± SD ($n = 3$). $^{*}P < 0.05$, compared with each Ub4. (F) Computational molecular docking of PtPT with UCHL5 and USP14 of the 26S proteasomes. The following data are shown: the structure of platinum pyrithione (L1); the structure of platinum pyrithione intermediate (L2); the binding modes of compound L2 at the active site of USP14; the binding models of compound L2 at the active site of UCHL5. (G) Active-site-directed labeling of proteasomal DUBs. Purified 26S proteasomes were treated with PtPT, NEM, or b-AP15, followed by labeling with HA-UbVS and immunoblotting for HA. One representative blot (E/left panel and G/upper panel) out of three independent experiments is shown and quantified by densitometric analysis (E/right panel and G/lower panel). Values are expressed as mean ± SD ($n = 3$). $^{*}P < 0.05$, compared with each 26S.

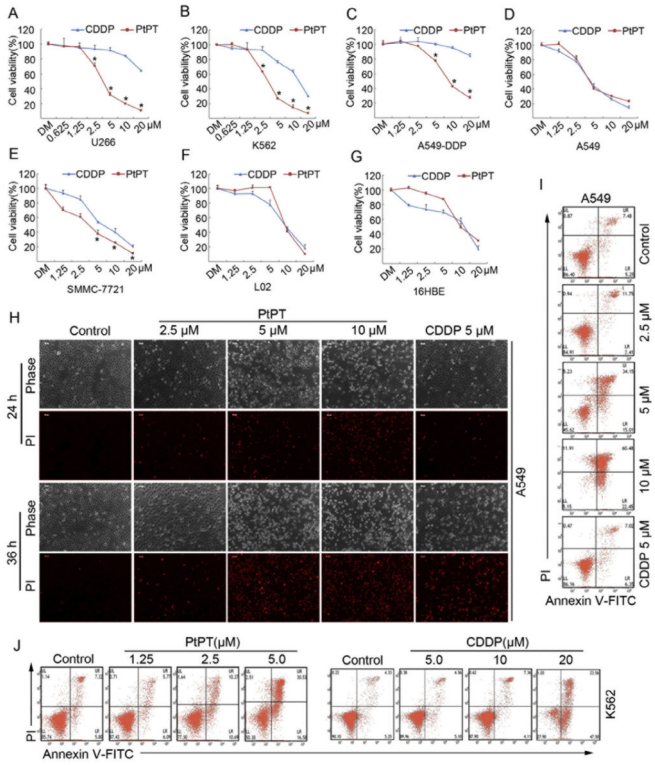

Fig. 6.

PtPT induces cytotoxicity in cultured cancer cells. (A–E) Cytotoxic curves in U266 (A), K562 (B), A549/DDP (C), A549 (D), SMMC-7721 (E) cells treated with increasing doses of PtPT or CDDP for 48 h. The cell viability was detected by MTS assay. Values are expressed as mean ± SD ($n = 3$). $^{*}P < 0.05$, compared with each CDDP. (F and G) LO2 (F) and 16HBE (G) cells were treated with escalating doses of PtPT or CDDP for 48 h, and cell viability was then detected by MTS assay. Values are expressed as mean ± SD ($n = 3$). $*P < 0.05$, compared with each CDDP. (H) PtPT induced cell death in A549 cells. A549 cells were treated with the indicated doses of PtPT or CDDP (5 μM), then PI was added to the cultured cells after 24 h treatment, and PI-positive staining was monitored under an inverted microscope and typical images are shown. (I and J) Apoptosis induction by PtPT in A549 and K562 cells. A549 and K562 cells were treated with the indicated doses of PtPT or CDDP (5 μM) for 24 h, apoptotic cells were detected with Annexin V–PI staining followed by flow cytometry.

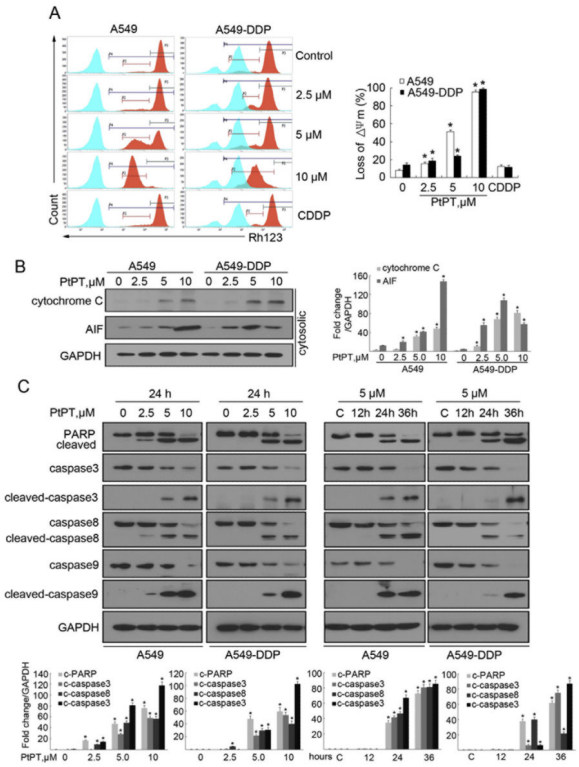

Fig. 7.

PtPT-induced apoptosis is associated with caspase activation. (A) PtPT induces down-regulation of mitochondrial membrane potential in A549 and A549/DDP cells. Cells were treated with the indicated dose of PtPT for 12 h, mitochondrial membrane potential was detected by rhodamine-123 staining followed by flow cytometry. Quantified analysis is given right. Values are expressed as mean ± SD ($n = 3$). $^{*}P < 0.05$, compared with each control. (B) PtPT induces cytochrome C and AIF release. A549 and A549/DDP cells were exposed to different doses of PtPT for 12 h, then cell cytoplasm were extracted by digitonin buffer and the released AIF and cytochrome C were detected by immunoblotting analysis. (C) PtPT induces cleavage of PARP, caspase-3, −8, −9 in A549 and A549/DDP cells. A549 and A549/DDP cells were treated with PtPT at various doses or for various times, PARP, and caspase-3, −8, −9 cleavage were analyzed by immunoblotting. GAPDH was detected as a loading control. One representative blot (B/left panel and C/upper panel) out of three independent experiments is shown and quantified by densitometric analysis (B/right panel and C/lower panel). Values are expressed as mean ± SD ($n = 3$). $^{*}P < 0.05$, compared with each control.

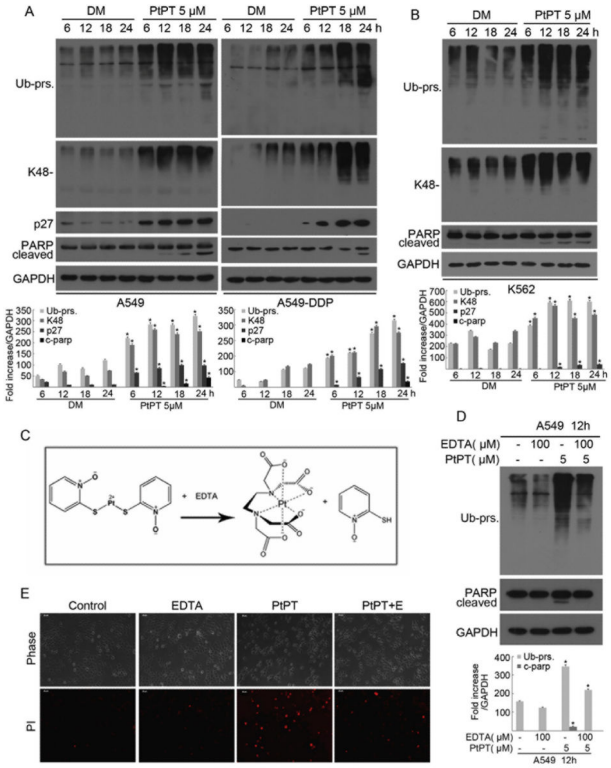

Fig. 8.

Proteasome inhibition is required for PtPT to induce apoptosis. (A and B) PtPT time-dependently induces proteasome function inhibition and apoptosis in cancer cells (A549, A549/DDP and K562). The cells in culture treated with PtPT (5 μM) were collected at the indicated time points for western blot analyses for ubiquitinated proteins including total ubiquitin conjugates (Ub-prs) and K48-linked polyubiquitins, p27, as well as cleaved PARP. (C) An illustration of the coordination of Pt with ethylenediaminetetraacetic acid (EDTA) to inactivate PtPT. (D and E) EDTA prevented most PtPT-induced proteasome inhibition and apoptosis. A549 cells were treated with PtPT with/without chelating agent EDTA (100 μM) for 12 h, total ubiquitin conjugates and PARP were detected with western blot analysis, and apoptosis cells were recorded with PI staining followed by imaging under fluorescence microscopy. One representative blot (A/B/D, upper panel) out of three independent experiments is shown and quantified by densitometric analysis (lower panel). Values are expressed as mean ± SD ($n = 3$). $^{*}P < 0.05$, compared with each control.

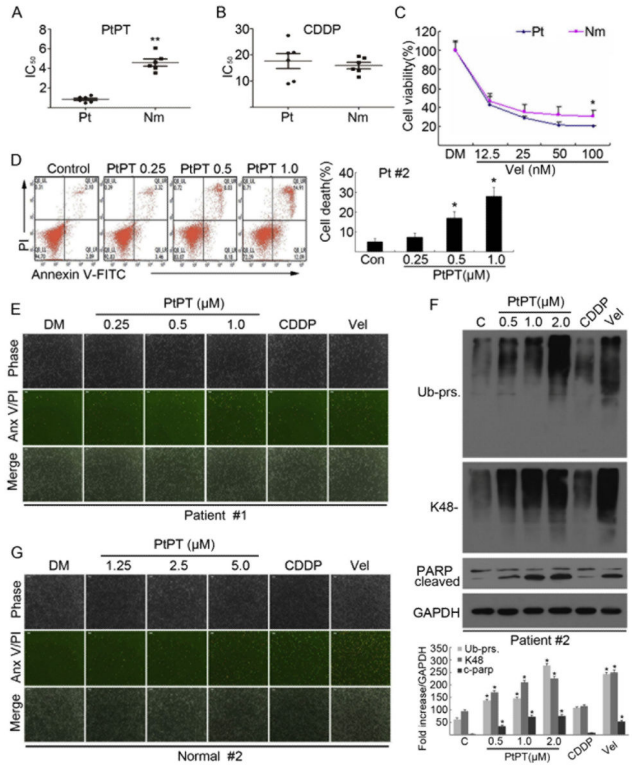

Fig. 9.

PtPT specifically induces cytotoxicity and proteasome inhibition in cancer cells from leukemia patients. (A–C) Cancer cells from 6 leukemia patients (Pt) and peripheral blood mononuclear cells from 6 healthy volunteers (Nm) were treated with PtPT at the indicated doses or with CDDP or Velcade (Vel) for 48 h, then the cell viability was detected by MTS assay. The scatter plots of the IC_{50} values of PtPT (A) and CDDP (B) in each group are shown. Cell viability with Vel treatment in each group is also shown (C). $n = 3$, Mean ± SD. $^{*}P < 0.05$, $^{**}P < 0.01$, compared with each control. (D) Cancer cells from patients were treated with increasing doses of PtPT for 24 h. Typical cell apoptosis from one sample (#2) was analyzed by flow cytometry and shown. Quantified analysis is given right. Values are expressed as mean ± SD ($n = 3$). $^{*}P < 0.05$, compared with each control. (E) Cancer cells from patients were incubated with PtPT at the indicated doses or with CDDP (10 μM) or Vel (50 nM) for 24 h, then cells were stained with Annexin V/PI and imaged under a fluorescent microscope (scale bar, 50 μm). Typical results from one sample (Patient #1) are shown. (F) Leukemia cells were incubated with PtPT at the indicated doses or with CDDP (10 μM) or Vel (50 nM) for 24 h, then ubiquitinated proteins and PARP were detected by western blot. Representative results from one sample (patient #2) are shown. One representative blot (F/upper panel) out of three independent experiments is shown and quantified by densitometric analysis (lower panel). Values are expressed as mean ± SD ($n = 3$). $^{*}P < 0.05$, compared with each control. (G) The peripheral mononuclear cells from normal human individuals were incubated with PtPT at the indicated doses or with CDDP (10 μM) or Vel (50 nM) for 24 h, then cells were stained with Annexin V/PI and imaged under a fluorescent microscope (scale bar, 50 μm). Representative images are shown.

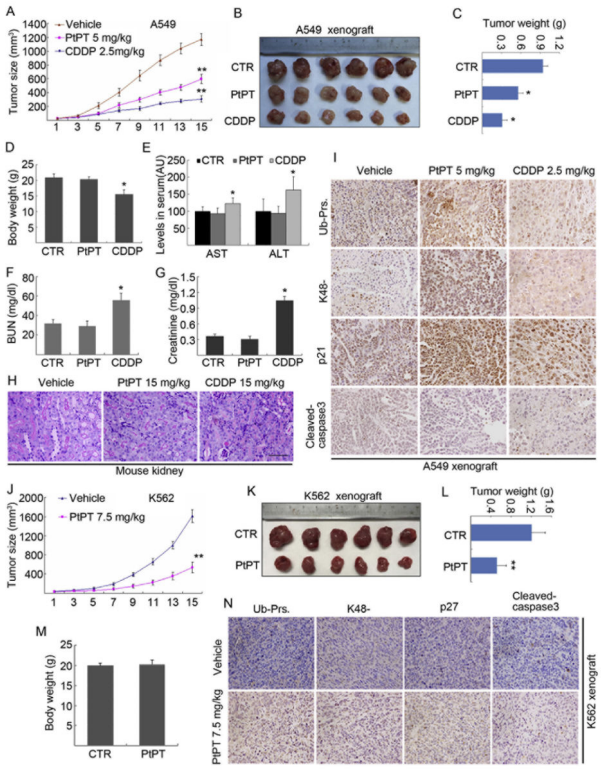

Fig. 10.

PtPT inhibits tumor growth and proteasome function *in vivo*. (A–D) BALB/c nude mice bearing A549 tumors were treated with vehicle or PtPT (5 mg/kg/day, i.p.) or CDDP (2.5 mg/kg/2 day, i.p.) for 15 days. Tumor size was recorded every other day. Tumor size (A), tumor images (B), tumor weight (C) and body weight (D) are shown. $n = 6$, mean ± SD. $^{*}P < 0.05$, $^{**}P < 0.01$, compared with each control. (E) Liver function was assessed by detecting serum AST and ALT. $n = 6$, mean ± SD. $^{*}P < 0.05$, compared with each control. AU, arbitrary unit. (F–H) BALB/c nude mice were treated with a single injection of vehicle, PtPT (15 mg/kg, i.p.) or CDDP (15 mg/kg/, i.p.), and sacrificed 4 days later. The graph showing the serum BUN (F) and creatinine (G) levels in each group. $^{*}P < 0.05$, compared to vehicle control ($n = 6$). Representative photomicrographs (200×) of mouse kidney sections with Periodic Acid Schiff staining are shown (H). (I) Representative immunohistochemical staining results are shown for total (Ub-prs) or K48-linked ubiquitin accumulation, proteasome substrate protein (p21), and cleaved caspase-3 in A549 tumor tissues from nude mice treated with vehicle, PtPT, or CDDP (200×). (J–M) BALB/c nude mice bearing K562 tumors were treated with either vehicle or PtPT (7.5 mg/kg/day, i.p.) for consecutive 15 days, Tumor size was recorded every other day. Tumor size (G), tumor images (H), tumor weight (I) and body weight (J) are shown. $n = 6$, mean ± SD. $^{**}P < 0.01$, compared with each control. (N) Representative images of immunohistochemical staining for total (Ub-prs), K48-linked ubiquitin accumulation, proteasome substrate protein (p27), and cleaved caspase-3 in tumor tissues from mice bearing K562 tumors treated with either vehicle or PtPT (200×).

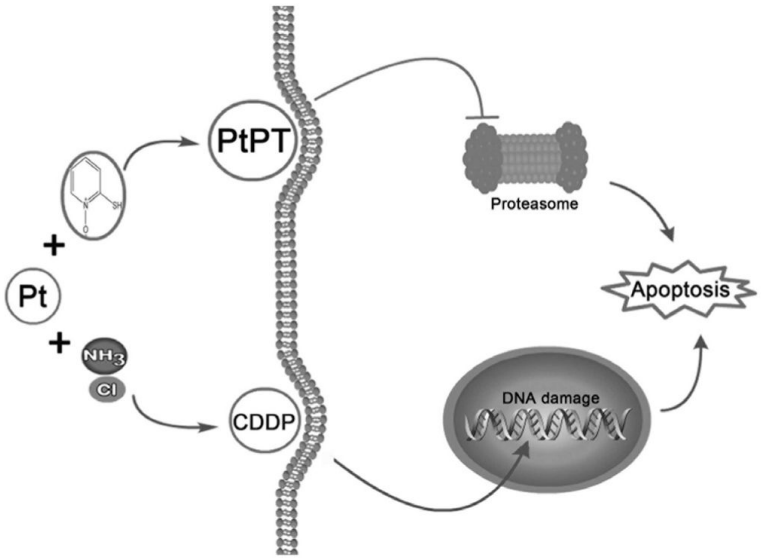

Fig. 11.

A schematic illustration of the biotarget of a novel platinum complex PtPT. Pt-based compounds target the different cellular components. CDDP but not PtPT interacts with DNA *via* covalent binding to induce DNA damage; conversely, PtPT but not CDDP targets proteasomal deubiquitinases. CDDP, cisplatin; PtPT, platinum pyrithione.